Hidden Kondo-Screening Revealed by Anomalous Hall Effect in $Fe_{3-\delta}GeTe_2$ Nanoflakes

Junjie Hou(候军杰)[1], Fan Chen(陈帆)[1], Mengying Ren(任梦颖)[1], Jianjun Tian(田建军)[2], Chaoyang Kang, (康朝阳)[2†] Han Jin, (金涵)[3‡] and Kai Wang(王凯) [1‡]

[1] *School of Physics and Electronics, Henan University, Kaifeng 475004, China*

[2] *Henan Key Laboratory of Quantum Materials and Quantum Energy, School of Quantum Information Future Technology, Henan University, Zhengzhou 450046, China*

[3] *Institute of Nano Biomedicine and Engineering & National Key Laboratory of Advanced Micro and Nano Manufacture Technology, School of Automation and Intelligent Sensing, Shanghai Jiao Tong University, Shanghai 200240, China*

The emergence of Kondo effect in Fe_3GeTe_2 (FGT) has attracted a lot of attentions due to a rare realization in 3*d* electron systems. However, the role of Fe-deficient on Kondo effect remains an open issue. Here, we focused on the studies of the anomalous Hall effect (AHE) for ideal stoichiometric and two different Fe-deficient FGT nanoflakes. Through the comparison of temperature dependence of spontaneous anomalous Hall resistance and coercive field among these FGT nanoflakes, unexpected reduction of anomalous Hall resistance and a kink behavior of coercive field below the Kondo crossover temperature in Fe-deficient samples well demonstrate the enhanced Kondo screening emerges due to Fe deficiency. Such an unconventional AHE could originate from the formation of enhanced local magnetism induced by the orbital-selective Mott correlation of Fe-I 3*d* electrons. This is consistent with the previous dynamical mean-field theoretical predictions, in which the distinct atomic environments of Fe-I and Fe -II give rise to dual role of local and itinerant magnetism respectively, thereby realizing the tuning of Kondo coupling through the change of electron filling. Our finding not only illustrate the role of Fe deficiency on the Kondo effect, but also provide a new insight to design the emergent quantum phenomenon.

Keywords: Anomalous Hall effect, Kondo screening, Fe_3GeTe_2, Fe deficiency

[†]Corresponding authors. E-mail: kangcy@vip.henu.edu.cn

[‡]Corresponding authors. E-mail: jinhan10@sjtu.edu.cn

[‡]Corresponding authors. E-mail: kai.wang@henu.edu.cn

1. Introduction

Anomalous hall effect (AHE) is widely regarded as a signature to identify a ferromagnetic metallic state, whereby the itinerant electrons possess spin polarization to generate the spontaneous Hall current through spin-orbit coupling.[1-4] Well-known empirical law, as expressed by Eq. (1)[2], derived through a perturbation expansion involving magnetization and the spin-orbit coupling (SOC) parameter.

$$R_{xy} \approx R_H H^{\rightarrow} + 4\pi R_s M^{\rightarrow} \quad (1)$$

Where the Hall resistance R_{xy} contains a contribution from the spontaneous magnetization ($M^{\rightarrow}$) in addition to the ordinary Hall effect. Therefore, a hard magnetic platform can build a connection between anomalous hall resistance and spontaneous magnetization due to a negligible ordinary Hall contribution. For a *f*-electron heavy fermion (HF) system, Local magnetic moment of *f*-electron is coherently screened by other itinerant electrons through Kondo effect to give rise to a heavy fermion state,[5,6] while the emergence of magnetism requires o break down coherent Kondo singlet state through Ruderman-Kittel-Kasuya-Yosida (RKKY) interaction.[7,8] Therefore, the HF state and magnetic order state in principle contradicts with each other,[5,9] which also implies that the AHE is absent in itinerant HF state due to the quench of ferromagnetism.[10,11]

Recently, Van der Waals metallic ferromagnet Fe_3GeTe_2 (FGT) illustrates a rare example to exhibit the coexistence of ferromagnetism and HF states[12] which benefits from the dual roles (itinerant and localized) of 3*d* electrons.[13] However, three important issues have not well understood up to now. Firstly, the localized or itinerant nature of magnetism is still in debate. Magnetization measurement[14] and the results of gate-tunable ferromagnetism[15] support the itinerant picture of magnetism, while recent angle-resolved photoemission spectroscopy (ARPES) study demonstrates that local magnetic moment plays an important role at low temperature instead of itinerant-stoner picture.[16] Secondly, although the neutron spectroscopy[17] and scanning tunneling spectroscopy measurements[18] well demonstrate the Kondo screening effect and HF behavior, the positive correlation between ferromagnetism and enhanced electron mass remains elusive[12], which is quite different from the *f*-electron system. Lastly, the role of Fe vacancy is not clear.

Magnetic properties of FGT are sensitive to doping[19]. Hole doping is reported to give rise of the reduction of ferromagnetic phase transition Cuire temperature T_c and magnetic anisotropy energy (MAE)[19], even probably leading to enhanced Kondo effect.[20] Dynamical mean-field theoretical (DMFT) calculations propose that two inequivalent Fe atoms due to different crystal field environments and electron fillings lead to distinct correlation effects of 3*d* electrons.[21-23] The introduction of Fe vacancy could give rise to the complex interactions of magnetism associated with possible Hund, Mott or Kondo physics.[20,23] However, there is no experimental evidence to elucidate the role of Fe vacancy, especially lacking of the direct comparison between ideal stochiometric FGT and Fe-deficient samples. Here, the AHE measurements are promising to clarify these issues through understanding the underlying interplay between itinerant ferromagnetism and Kondo correlation induced magnetic screening.

In this study, we focused on the AHE investigations for ideal stoichiometric and two different Fe-deficient FGT nanoflakes. The hard magnetic behaviors are observed for all the nanoflakes due to enhanced MAE in contrast to their bulk counterparts, furthermore, Fe deficiency reduces the perpendicular MAE, giving rise to the decrease of cercive field in deficient nanoflakes. Intriguingly, anomalous Hall resistance extracted by zero field AHE in deficient nanoflakes shows an unusual temperature evolution, and unexpected reduction of AHE occurs below Kondo crossover temperature, which can be attributed to Kondo screening between local and itinerant magnetic moment of 3*d* electrons. In addition, coercive field shows a kink behavior within the temperature regime, which also well demonstrate the competing correlation between local and itinerant roles due to antiferromagnetic-type coupling. Furthermore, robust AHE and rapid increase of coercive field at lower temperature indicates the coexistence of local ferromagnetism and HF states. Our findings well demonstrate the enhanced Kondo screening emerges in Fe deficient FGT. It could originate from the enhanced role of local magnetic magnetism due to the change of electron filling, which is consistent with the Dynamical Mean-field theoretical predictions.

2. Methods

2.1. The growth of single-crystal

We employed two different methods to synthesize three bulk FGT single crystals. Among them, two samples with relatively fewer Fe defects were prepared using the chemical vapor transport (CVT) method. The detailed synthesis procedure is as follows. First, iron powder (99.9%), germanium powder (99.99%), and tellurium powder (99.99%) were mixed in a stoichiometric ratio of 3:1:2 and 2.9:1:2 respectively. The homogeneous mixture was then placed in a quartz tube filled with iodine (2 mg/cm) as a transport agent. The quartz tube was vacuum-sealed and subjected to heat treatment in a dual-zone tube furnace with a temperature gradient of 750–700℃ for 7 days. After the heat treatment, the furnace was allowed to cool naturally to room temperature to yield silver-colored plate-like $Fe_{3-\delta}GeTe_2$ single crystals. The third sample, which contains a higher density of Fe defects, was synthesized via a self-flux method, with specific steps outlined below. Fe (99.99%), Ge (99.99%), and Te (99.99%) powders with the 2:1:4 mol ratio were fully mixed. The mixture was then placed into an alumina crucible, sealed in a quartz tube with 10^{-3} Pa Ar pressure, heated slowly to 1100℃, kept at 1100℃ for 12 h, and cooled to 600℃ over 150 h. The crucible was quenched in cold water after the full heating process. Shiny, cleanable $Fe_{3-\delta}GeTe_2$ single crystals could be picked out from the product.

2.2. Electrode processing

Hall-bar electrodes were prepared using ultraviolet lithography combined with vacuum deposition for more precise electrical transport measurements. Initially, a standard Hall Bar electrode of Cr(5 nm)/Au(30 nm) with dimensions of 2 μm×8 μm was fabricated on a Si/SiO_2(582 nm) substrate using an ultraviolet lithography machine (URE-2000). Subsequently, high-quality Fe_3GeTe_2 single crystals grown using the chemical vapor transport method were cleaved in a glove box filled with Ar gas (H_2O and O_2 concentrations below 0.01 ppm). Suitable thin layers of Fe_3GeTe_2 were selected under an optical microscope, extracted, and transferred using PDMS. A two-dimensional material transfer platform was used to precisely place the Fe_3GeTe_2 flake at the center of the Hall Bar, and a larger layer of hexagonal boron nitride (h-BN) was transferred on top as a protective layer to prevent oxidation or hydrolysis of the $Fe_{3-\delta}GeTe_2$ flake. Finally, the entire device was annealed at 180℃ for 20 minutes to ensure full contact between the sample and the electrodes and to eliminate any potential bubbles.

2.3. Characterization.

The magnetic properties of the $Fe_{3-\delta}GeTe_2$ single crystals were tested using a vibrating sample magnetometer (VSM), and the electrical transport properties of the samples were measured using a comprehensive physical property measurement system (PPMS-9 EverCool) produced by Quantum Design. Considering the potential asymmetry in the fabricated Hall bar, the measured Hall resistance may include contributions from longitudinal magnetoresistance. Hence, the measured data need to be symmetrized $(R_{xy}(+\mu_0 H)-R_{xy}(-\mu_0 H))/2$ to remove the contribution of longitudinal magnetoresistance.

3.Results and discussion

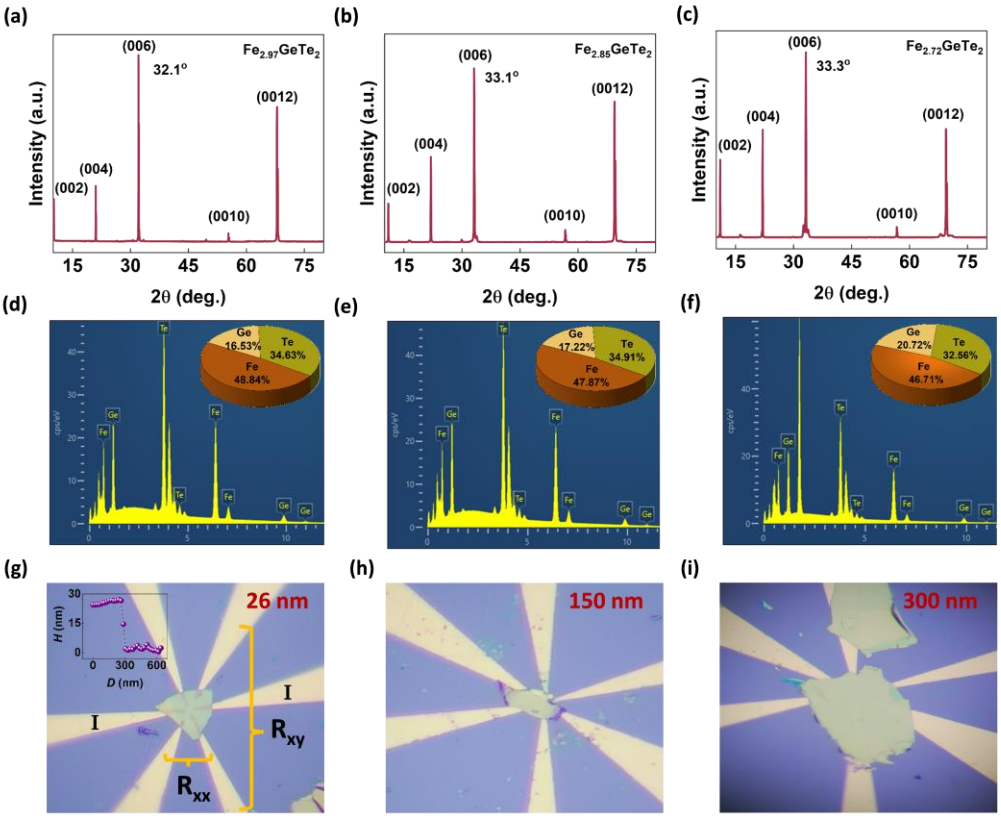


FIG. 1 (a)(b)(c) XRD patterns of FGT with three different Fe contents; (d)(e)(f) EDS spectra of FGT with three different Fe contents, with insets showing the calculated stoichiometric ratios; (g)(h)(i) Optical microscopy images of nanosheets with different thicknesses, mechanically exfoliated from Fe_3GeTe_2 single crystals and placed on Hall bar electrodes (nanosheets with different thicknesses were also obtained from the other two types of single crystals).

We synthesized a series of $Fe_{3-\delta}GeTe_2$ single crystals with varying Fe content . X-ray diffraction (XRD) patterns (Fig. 1(a)-1(c)) show that all three single crystals exhibit (00L) diffraction peaks, indicating that they all possess high crystalline quality. Furthermore, as the Fe vacancy concentration increases, their main peak ((006)) shifts slightly toward higher 2θ angles, suggesting a slight decrease in the lattice constant. Energy dispersive spectroscopy (EDS) (Fig. 1(d)-1(f)) was employed to determine the elemental composition, and the atomic ratios of Fe, Ge, and Te were calculated based on the characteristic peak intensities, as shown in the insets of Fig. S2. The chemical formulas of the three samples were determined to be $Fe_{2.97}GeTe_2$, $Fe_{2.85}GeTe_2$, and $Fe_{2.72}GeTe_2$ respectively. In addition, we exfoliated nanosheets of different thicknesses from the bulk single crystals for electrical transport measurements; representative images are shown in Fig. 1(g)-1(i).

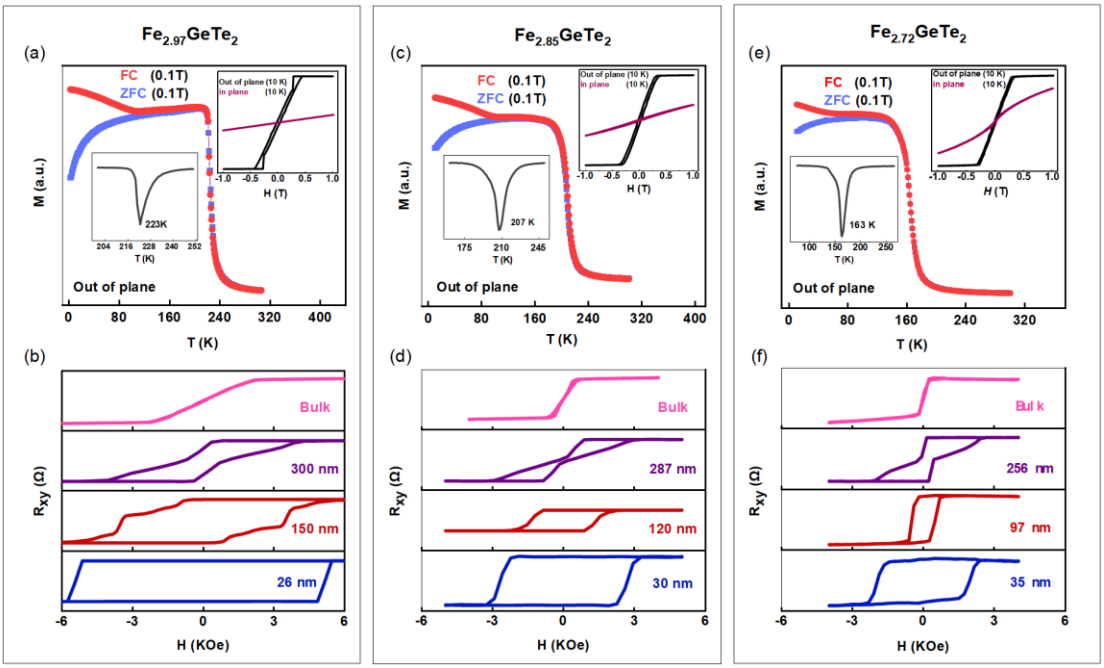


FIG. 2 (a) (c) (e) The zero-field-cooled (ZFC) and field-cooled (FC) magnetization curves of FGT single crystals ((a)$Fe_{2.97}GeTe_2$ (c)$Fe_{2.85}GeTe_2$ (e)$Fe_{2.72}GeTe_2$) along the out-of-plane (c-axis) direction. The insets show the derivative ZFC curves and the out-of-plane and in-plane *MH* curves of an FGT single crystal at a temperature of 10 K. (b) (d) (f) R_{xy}-*H* curves for FGT nanoflakes ((b)$Fe_{2.97}GeTe_2$ (d)$Fe_{2.85}GeTe_2$ (f)$Fe_{2.72}GeTe_2$)of various thicknesses at 2 K.

Magnetic measurements (Fig. 2(a), (c), (e), and insets) indicates that all samples exhibit pronounced perpendicular magnetic anisotropy (PMA) and undergo a ferromagnetic (FM) phase transition from a paramagnetic phase of high temperature upon cooling. The derivative of the out-of-plane magnetization-

temperature (*M-T*) curves (insets of Fig. 2(a), (c), (e)) shows a systematic decrease in the Curie temperature (T_c) with increasing Fe deficiency. The T_c values of the three samples decrease from 223 K to 163 K with increasing Fe deficiency, which is consistent with previous reports, in which the T_c of $Fe_{3-\delta}GeTe_2$ was found to range from 230 K to 140 K depending on the Fe content [24]. In addition, Fe deficiency also affects the PMA, as shown in the inset of Fig. 2(a), (c), (e), ab-plane magnetization-field (*M-H*) curves in Fe-deficient samples are more readily towards saturation compared to ideally stoichiometric FGT, which indicates PMA energy is weaken due to the increase of Fe deficiency. To further investigate thickness-dependent transport properties, we mechanically exfoliated the single crystals into nanosheets of varying thicknesses and performed direct-current (DC) magneto transport measurements at 2 K. The applied magnetic field was perpendicular to the surface of the samples. The Hall resistance versus magnetic field curves (R_{xy}-*H*) (Fig. 2(b), (d), (f)) demonstrate similar thickness-dependent behavior across all samples: Bulk crystals exhibit typical soft magnetic characteristics; Intermediate-thickness nanosheets (100-300 nm) display two-step hysteresis loops with distinct coercive fields, suggesting the presence of complex multi-domain structures; Ultrathin nanosheets (<50 nm) exhibit nearly square hysteresis loops, indicative of single-domain behavior ,consistent with hard magnetic properties.[25] This thickness-dependent magnetic behavior has been well explained as the consequence of enhanced PMA energy as decreasing thickness in previous studies. In addition to that, we find coercive field is also reduced due to the increasing of Fe deficiencies through making the comparison among these ultrathin nanosheets at low temperature.

Although coercive field is sensitive to the thickness, a clear reduction of coercive field from about 0.6 to 0.3 T suggests that deficient concentrations underlying change the PMA, as discussed aforementioned for bulk samples, such a reduction also can be reasonably understood as the changes of PMA induced by Fe deficiency.

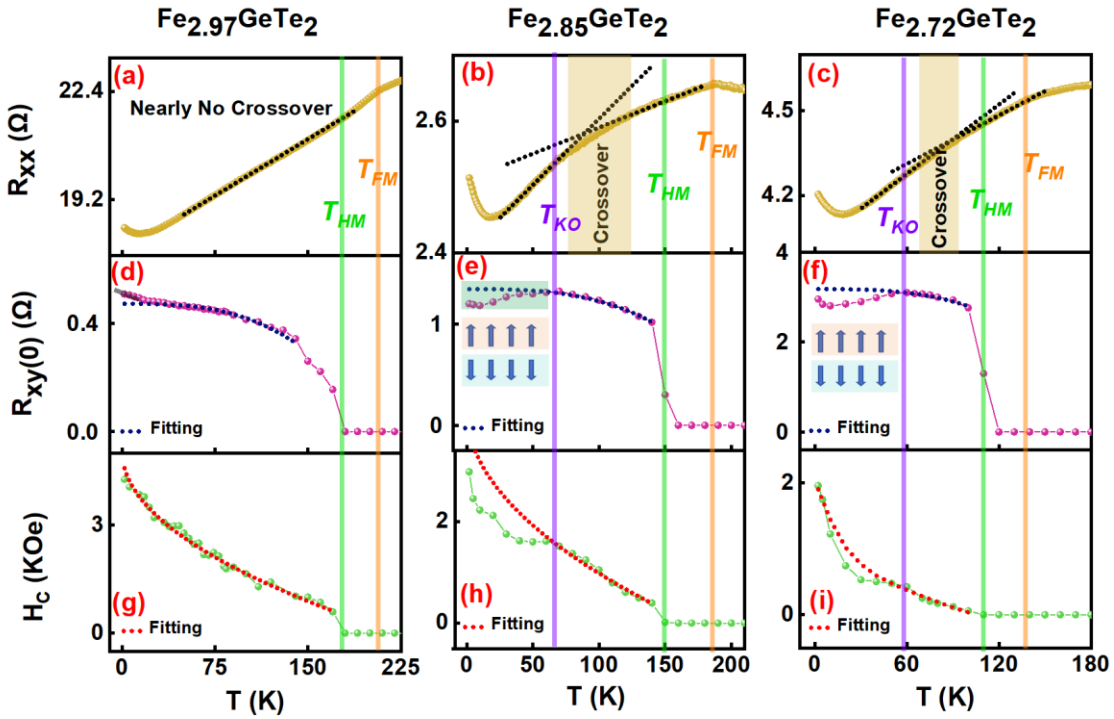


FIG.3 (a) (b) (c) R_{xx}-T and their fitting curves of Fe_3-$_\delta GeTe_2$ nanoflakes. (d) (e) (f) $R_{xy}(0)$-T and their fitting curves of Fe_3-$_\delta GeTe_2$ nanoflakes. (g) (h) (i) H_c-T and their fitting curves of Fe_3-$_\delta GeTe_2$ nanoflakes.

In order to give more insights for complex magnetic response, we systematically investigate the temperature evolution of AHE in three Fe_3-$_\delta GeTe_2$ nanoflakes with different Fe deficient concentration, each approximately 30 nm thick and exhibiting square-like hysteresis loops. As shown in Supplemental FigS1. (a)-(c) displays their R_{xy}-H curves at various temperatures. All three nanosheets exhibit nearly square-shaped hysteresis loops at low temperatures. Upon cooling down, the coercive field gradually increases, followed by a transition from soft magnetic behavior to hard magnetism. For a hard magnetic response, the zero-field anomalous Hall resistance ($R_{xy}(0)$) coercive field (H_c) can be well extracted, subsequently plotting their temperature-dependent variations ($R_{xy}(0)$-T and H_c-T curves). Longitudinal resistance versus temperature curves (R_{xx}-T), as presented in Figs. 3(a), (b), and (c). The R_{xx}-T curves of all three Fe_3-$_\delta GeTe_2$ nanoflakes with different Fe concentrations exhibited characteristic metallic behavior, with observed kinks corresponding to their respective ferromagnetic transition temperatures, labelled by vertical FM orange lines. Below T_c, in the ideally stoichiometric $Fe_{2.97}GeTe_2$ nanosheets, R_{xx}-T shows a single linear temperature dependence within the metallic temperature regimes. In contrast to that of other two deficient

nanoflakes, two distinct linear temperature response allows one to recognize a crossover region, marked by bold orange lines. Additionally, the green line is defined by the emergence of hard magnetism in AHE, as shown in Figs. 3(d), (e), and (f), below $T_{HM,}$ the $R_{xy}(0)$-T can be well fitted by spin-wave theory ($M \propto a + b(\frac{k_B T}{2J_S})^{3/2}$), in $Fe_{2.97}GeTe_2$ nanosheets, the results have been discussed in previous literatures, in particular, slight deviation from spin-wave theory below around 20 K has been well demonstrated as the enhanced AHE due to crystalline symmetry protected Berry curvature.[26] Therefore, below around 20 K, the $R_{xy}(0)$ is beyond the empirical relationships determined by Eq. (1), while at our interested temperature regimes from 20 K to crossover temperature T_{ko}, $R_{xy}(0)$ is proportional to magnetization of out of plane. As shown in Figs. 3(d), the increase of M_z as temperature decreasing leads to gradually enhanced $R_{xy}(0)$. Specifically, due to reduced spin-wave excitation upon cooling down, the magnetization tends to saturate when the system is close to the ground state. However, as shown in Figs. 3(e), and (f), a clear reduction of $R_{xy}(0)$ occurs below $T_{ko,}$ which indicates that itinerant

M_z is partially screened. Obviously, such a reduction is hard to reconcile within the framework of conventional FM state, in which the M_z always increases as reduced thermal fluctuations. Here, it is necessary to note that the square-shaped hard magnetic manifestation can rule out the possibilities of various spin textures, such as skyrmions and multi-domain inhomogeneous ferromagnetism. Therefore, a reasonable explanation is that the reduced itinerant M_z is induced by antiferromagnetic-type Kondo-like coupling, which also implies that localized magnetic role requires to develop below T_{ko}. In addition, within the temperature regimes, neutron and STM investigations demonstrate that the system undergoes a coherent-incoherent crossover in the FM state, manifested as Kondo-lattice behavior.[17,18] Combining with our current temperature anomaly of $R_{xy}(0)$ in $Fe_{2.85}GeTe_2$ and $Fe_{2.72}GeTe_2$, we can conclude that localized and itinerant magnetism coexists, and Fe deficiencies give rise to enhanced Kondo-like screening, thereby leading to reduced itinerant magnetism, manifesting as the reduction of $R_{xy}(0)$.

A widely employed anisotropic Heisenberg Hamiltonian in the presence of strong magnetic anisotropy is as follows:

$$H = \sum_{i,j} J_{ij} \boldsymbol{S}_i \cdot \boldsymbol{S}_j + \sum_i A(S_i^z)^2$$

where $\boldsymbol{S}_i$ is the spin operator on site i, and J_{ij} denotes the exchange coupling on site i and j; A is the single-ion perpendicular magneto-crystalline anisotropy energy arising from spin-orbital coupling. Although the current magnetism refers to complex interplay between itinerant and localized magnetism, the anisotropic Heisenberg model is believed to be sufficient to qualitatively understand magnetic properties of FGT. Based on the model, coercive field (H_c) can be determined by magnetic anisotropy energy and spontaneous magnetization induced by spin-exchange interactions, while for a certain FGT nanoflake, the temperature dependence of H_c is dominated by spontaneous magnetization. Here, due to the coexistence of itinerant and localized magnetism, we marked M_{tot} represent the total magnetization. As shown in Figs. 3(g) (h), and (i), the temperature dependence of H_c is fitted by using $Hc \propto \mathrm{Mtot} \propto a + b(\frac{k_B T}{2J_S})^{1/2}$, in which the power-law exponent is different from the prediction of spin-wave theory, coincide with the mean-field prediction below ferromagnetic phase transition temperature. Due to the common effect of magnetic anisotropy energy and spin-exchange interactions, enabling the precise prediction for the temperature dependence of magnetization become difficult. However, a clear kink behavior of H_c in $Fe_{2.85}GeTe_2$ and $Fe_{2.72}GeTe_2$ can be well recognized, which is absent in $Fe_{2.97}GeTe_2$ nanosheets. Considering Kondo screening effect in the temperature regime, the kink behavior can be naturally attributed to the competing correlation between itinerant and localized magnetism. Furthermore, H_c shows a rapid increase below the competing temperature regimes, which indicates that the total magnetization is still robust although Kondo screening is enhanced at lower temperatures. Consequently, Ferromagnetism and Heavy fermion behavior is positively correlated, both enhanced at low temperatures. Moreover, (R_{xx}), $R_{xy}(0)$ and (H_c) of $Fe_{2.97}GeTe_2$ within the interested temperature regimes do not show a clear anomaly compared to other two deficient samples, which suggest the important role of Fe deficiency for magnetic properties. In

addition to that, as shown in Fig.S2, the dc conductivity below around 20 K shows a logarithmic temperature dependence, which is consistent with the picture of Kondo localization. Intriguingly, the two deficient samples exhibit a much larger coefficient than that of the ideally- stoichiometric sample, which is consistent with enhanced Kondo screening in Fe-deficient samples.

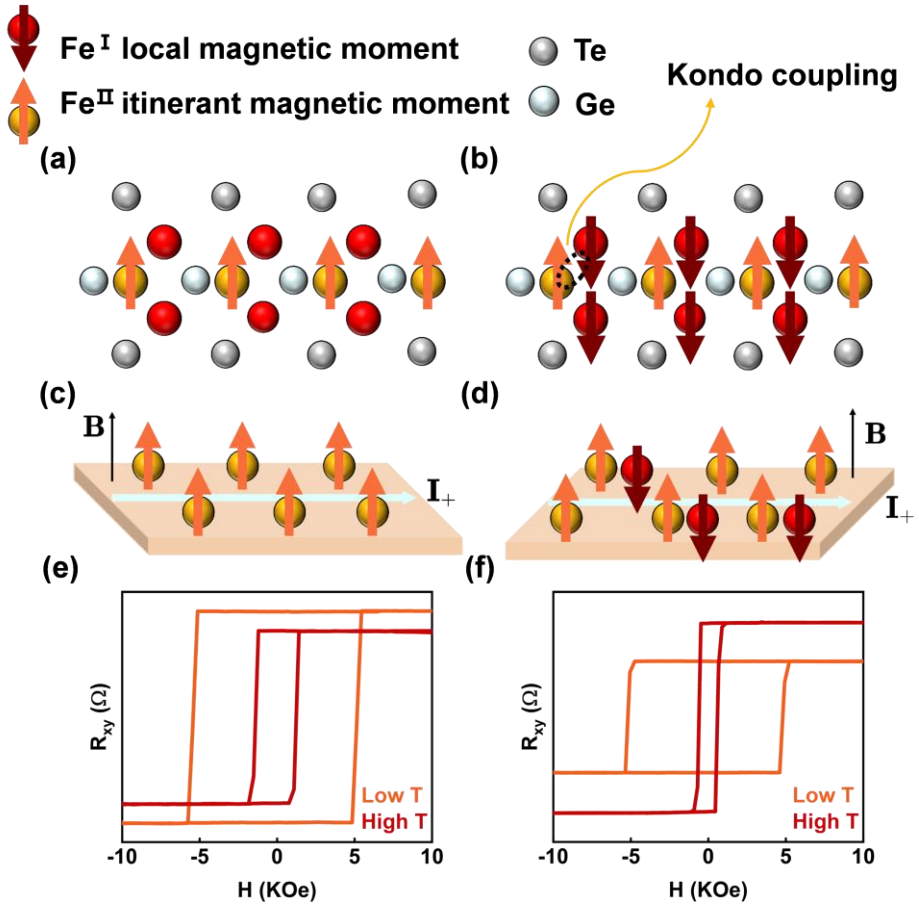


FIG.4 Schematic illustration of Kondo coupling on the anomalous Hall effect in FGT. (a) (b) Crystal structure and magnetic moment configuration: (a) In the absence of Kondo coupling, Fe itinerant magnetism develops to give rise to AHE (b) Onset of Kondo coupling, the local magnetism of Fe-I sites forms Kondo singlets with itinerant Fe-II electrons (indicated by dashed circles). (c) (d) schematic diagram of AHE: (c) AHE response in conventional itinerant metals. (d) With Kondo coupling, the unconventional screening of AHE (e) (f) The manifestations of Anomalous Hall resistance R_{xy} as a function of magnetic field H: (e) typical ferromagnetic behavior, as temperature decreases, the magnitude of R_{xy} increases. (f) With Kondo coupling, as temperature decreases, the Kondo screening effect becomes more pronounced at low temperatures, causing the magnitude of R_{xy} to decrease compared to the high-temperature curve, reflecting a strong suppression of the AHE by the Kondo effect.

The previous dynamical mean-field theoretical (DMFT) predictions[21-23] focus on the distinct correlated role of 3*d* electrons of Fe-I and Fe-II due to the difference of their atomic environment and electronic filling, as shown in Figs.4(a,b). specifically, Taek Jung Kim et al,[21] suggest that the background state of FGT is Fe-site differentiated Hund metal, in which 3*d* electrons of Fe-I and Fe-II are both dominated by Hund coupling, thus, in this picture, it is hard to expect the emergence of local magnetism. While, Yuanji Xu, et al, [23] suggest the 3*d* electron of Fe-I is close to half-filling $3d^5$ case, in which Hund enhanced orbital-selective Mott correlation predominates the electronic behavior, thereby gives rise to local ferromagnetism. 3*d* electrons of Fe-II are still dominated by Hund coupling, which naturally leads to itinerant magnetic moment. Therefore, our current results support such a picture. Spontaneous Hall resistance can identify the spin polarized itinerant carriers[25], as shown in Figs. 4(c,d), that is, the role of itinerant magnetic moment can give rise to AHE. Accordingly, the clear reduction of spontaneous Hall resistance in Fe-deficient samples (See Figs. 4(f)) well demonstrates the Kondo like coupling between local and itinerant magnetism.[20] Furthermore, the kink observations of coercive field also point to the development of local magnetic moment, Kondo coupling causes the anomaly of total magnetization.[12]

4. Conclusion

In summary, we investigated the thickness and temperature dependence of AHE for ideal stochiometric and two different Fe-deficient FGT samples. The prominent findings focus on the unexpected anomalous Hall resistance $R_{xy}(0)$ and the kink behavior of coercive field H_c, in which the reductions of $R_{xy}(0)$ and the kink anomaly of H_c well demonstrate the enhance Kondo screening in Fe-deficient samples. Such a deficient effect can be understood as the consequence of complex correlated interplay between Fe-I orbital selective Mott correlations and Fe-II Hund coupling. Such a picture is consistent with the previous DMFT predictions. These finding provide a new insight to study and design emergent quantum phenomenon related to Kondo effect.

Acknowledgments

This work was supported by the National Natural Science Foundation of China (Grant No.11405045) and Natural Science Foundation of Henan Province (No. 252300421482 and No. 242300421378).

References

[1] Karplus R and Luttinger J M 1954 *Phys. Rev.* **95** 1154.

[2] Hurd C M 1972 *The Hall Effect in Metals and Alloys* (New York: Plenum Press) p. 50

[3] Onoda S, Sugimoto N and Nagaosa N 2007 arXiv:0712.0210.

[4] Nagaosa N, Sinova J, Onoda S, MacDonald A H and Ong N P 2010 *Rev. Mod. Phys.* **82** 1539.

[5] Doniach S 1977 *Phys. B+C* **91** 231.

[6] Stewart S G R 1984 *Rev. Mod. Phys.* **56** 755.

[7] Ruderman M A and Kittel C 1954 *Phys. Rev.* **96** 99;Kasuya T 1956 *Theor. Phys.* **16** 45; Yosida K 1957 *Phys. Rev.* **106** 893.

[8] Si Q, Rabello S, Ingersent K and Smith J L 2001 *Nature* **413** 804.

[9] Stewart G R 2001 *Rev. Mod. Phys.* **73** 797.

[10] Kontani H and Yamada K 1994 *J. Phys. Soc. Jpn.* **63** 2627.

[11] Kirchner S, Paschen S, Chen Q Y, Wirth S, Feng D L, Thompson J D and Si Q 2020 *Rev. Mod. Phys.* **92** 011002.

[12] Zhang Y, Lu H Y, Zhu X G, Tan S Y, Feng W, Liu Q, Zhang W, Chen Q Y, Liu Y, Luo X B, Xie D H, Luo L Z, Zhang Z J and Lai X C 2018 *Sci. Adv.* **4** eaao6791.

[13] Fei Z Y, Huang B, Malinowski P, Wang W B, Song T C, Sanchez J, Yao W, Xiao D, Zhu X Y, May A F, Wu W D, Cobden D H, Chu J H and Xu X D 2018 *Nat. Mater.* **17** 778.

[14] Chen B, Yang J H, Wang H D, Imai M, Ohta H, Michioka C, Yoshimura K and Fang M H 2013 *J. Phys. Soc. Jpn.* **82** 124711.

[15] Deng Y J, Yu Y J, Song Y C, Zhang J Z, Wang N Z, Sun Z Y, Yi Y F, Wu Y Z, Wu S W, Zhu J Y, Wang J, Chen X H and Zhang Y B 2018 *Nature* **563** 94.

[16] Xu X, Li Y W, Duan S R, Zhang S L, Chen Y J, Kang L, Liang A J, Chen C, Xia W, Xu Y, Malinowski P, Xu X D, Chu J H, Li G, Guo Y F , Liu Z K, Yang L X and Chen Y L 2020 *Phys. Rev. B* **101** 201104.

[17] Bao S, Wang W, Shangguan Y Y, Cai Z W, Dong Z Y, Huang Z T, Si W D, Ma Z, Kajimoto R, Ikeuchi K, Yano S, Yu S L, Wan X G, Li J X and Wen J S 2022 *Phys. Rev. X* **12** 011022.

[18] Nguyen G D, Lee J, Berlijn T, Zou Q, Hus S M, Park J, Gai Z, Lee C and Li A P 2018 *Phys. Rev. B* **97** 014425.

[19] Park S Y, Kim D S, Liu Y, Hwang J, Kim Y H, Kim W D, Kim J Y, Petrovic C, Hwang C, Mo S K, Kim H J, Min B C, Koo H C, Chang J, Jang C, Choi J W and Ryu H 2019 *Nano Lett.* **20** 95.

[20] Zhao M T, Chen B B, Xi Y L, Zhao Y Y, Xu H, Zhang H R, Cheng N Y, Feng H F, Zhuang J C, Pan F, Xu X, Hao W C, Li W, Zhou S, Dou S X and Du Y 2021 *Nano Lett.* **21** 6117.

[21] Kim T J, Ryee S and Han M J 2022 *Mater.* **8** 245.

[22] Zhu J X, Janoschek M, Chaves D S, Cezar J C, Durakiewicz T, Ronning F, Sassa Y, Mansson M, Scott B L, Wakeham N, Bauer E D and Thompson J D 2016 *Phys. Rev. B* **93** 144404.

[23] Xu Y J, Wang Y C, Jin X T, Liu H F, Liu Y, Song H F and Tian F Y 2024 *Commun. Phys.* **7** 381.

[24] May A F, Calder S, Cantoni C, Cao H B and McGuire M A 2016 *Phys. Rev. B* **93** 014411.

[25] Tan C, Lee J, Jung S G, Park T, Albarakati S, Partridge J, Field M R, McCulloch D G, Wang L and Lee C 2018 *Nat. Commun.* **9** 1554.

[26] Liu C L, Shen Z T, Kang C Y, Han Y Y, Tian J J, Ying T P, Zhang W F and Wang K 2025 *Phys. Rev. B* **111** 134425.